Atmospheric boundary layer characteristics from Ceilometer measurements part 2: application to London's urban boundary layer

Received: 15 November 2017 | Revised: 15 March 2018 | Accepted: 22 March 2018

DOI: 10.1002/qj.3298

RESEARCH ARTICLE

Quarterly Journal of the Royal Meteorological Society RMetS

Atmospheric boundary-layer characteristics from ceilometer measurements. Part 2: Application to London's urban boundary layer

Simone Kotthaus[1,2] | C. Sue B. Grimmond[1]

[1]Department of Meteorology, University of Reading, Reading, UK
[2]Institute Pierre Simon Laplace, Centre National de la Recherche Scientifique, École Polytechnique, 91128 Palaiseau, France

Correspondence
Simone Kotthaus, Department of Meteorology, University of Reading, PO Box 217 Reading, RG6 6AH, UK.
Email: s.kotthaus@reading.ac.uk

Funding information
EU FP7, BRIDGE. EU H2020, URBANFLUXES. NERC, ClearfLo (NE/H003231/1). NERC, APHH-China (NE/N00/00X/1), Newton Fund/Met Office, CSSP-China, King's College London, University of Reading.

Long-term measurements of mixed layer height (Z_{ML}) are possible with advances in detecting Z_{ML} based on Automatic Lidars and Ceilometers (ALC) observations. Six years of ALC measurements in central London are analysed using the CABAM ("Characterising the Atmospheric Boundary layer (ABL) based on ALC Measurements") algorithm which provides Z_{ML} and an ABL classification by cloud cover and type. The boundary-layer dynamics are shown to respond to day-length, cloud cover and cloud type. Seasonal median daily maxima range from 707 m (stratiform clouds) to 1704 m (days with convective boundary-layer clouds following a clear night). A common approach to ABL classification and clear definition of key Z_{ML}-indicators can facilitate inter-city comparison. A simple parametrisation based on empirical coefficients derived from the London measurements is proposed to generalise the description of diurnal and seasonal variations in Z_{ML}, including cloud conditions. This has the potential to aid improved understanding of the complex relations between surface air quality and boundary-layer dynamics.

KEYWORDS
ABL, ALC, boundary-layer clouds, CABAM, ceilometer, mixed layer height, urban boundary layer

1 | INTRODUCTION

With air pollution responsible for about 467,000 premature deaths in Europe annually (EEA, 2016), health problems from exposure are estimated to be more than £20bn p.a. in the United Kingdom alone (TRCP, 2016). In urban areas, where both population density and pollution from road traffic are high, air quality is a major concern, with much effort directed to reduce emissions and exposure (GLA, 2016). Detailed understanding of the physical and chemical dynamics in the near-surface atmosphere is key to the development of guidelines and efficient monitoring (Mittal *et al.,* 2016).

Abbreviations: Δt_{ET}, duration of evening transition; Δt_{MT}, duration of morning transition; Δt_{noc}, duration between evening transition and time of minimum Z_{ML}; Δz, height difference; Δz_{MT}, dilution height during morning transition; Δz_{noc}, nocturnal reduction height; ABL, atmospheric boundary layer; agl, above ground level; ALC, automatic lidars and ceilometers; AMDAR, Aircraft Meteorological Data Relay; CABAM, Characterising the Atmospheric Boundary layer based on ALC Measurements; CBH, cloud base height; Cu, cumulus cloud, also ABL class of days dominated by Cu; day_{SR}, 24 hr periods centred on sunrise; DR, nocturnal decay rate; ET, evening transition; *f*, relative percentage; GR, growth rate; H_{day}, duration of day; H_{night}, duration of night; IQR, inter-quartile range; ML, mixed layer; MN, midnight; MT, morning transition; PM, particulate matter; SN, solar noon; SR, sunrise; SS, sunset.; St, stratiform cloud, also ABL class of days dominated by St; *t,* time; $t1_{ET}$, beginning of evening transition; $t1_{MT}$, beginning of morning transition; $t2_{ET}$, end of evening transition; $t2_{MT}$, end of morning transition; t_{max}, time of maximum mixed layer height; t_{min}, time of minimum mixed layer height; VOC, volatile organic compound; z, height above ground; $z1_{ET}$, mixed layer height at beginning of evening transition; $z1_{MT}$, mixed layer height at beginning of morning transition; $z2_{ET}$, mixed layer height at end of evening transition; $z2_{MT}$, mixed layer height at end of morning transition; z_{max}, maximum mixed layer height; z_{min}, minimum mixed layer height; Z_{ML}, mixed layer height.

Interpretation of pollutant concentrations observed near the surface requires insights into atmospheric boundary-layer (ABL) dynamics (e.g. Curci *et al.,* 2015; Tang *et al.,* 2016), given that the height (Z_{ML}) of the mixed layer (ML) determines the volume within which aerosols, greenhouse gases and moisture emitted at the surface are diluted. On days with little cloud cover and calm winds, air pollution levels can correlate negatively with Z_{ML}, as shown e.g. for particulate matter (PM: Münkel *et al.,* 2007; Schäfer *et al.*, 2012; Tang *et al.,* 2016), volatile organic compounds (VOCs: Wagner and Kuttler, 2014), and NO_x (Wagner and Schäfer, 2017). These "text-book" days often have a shallow nocturnal layer that grows into a convective mixed-layer which comprises the whole depth of the ABL in the afternoon. Through entrainment, clear air from the free atmosphere or potentially aerosol-laden air from residual layers may be brought into the ML and contribute to ground-level conditions. For example, aerosols present in the residual layer for several days above Milan undergo extended chemical reactions so that secondary aerosols eventually mixed down may account for 40% of surface $PM_{2.5}$ (Curci *et al.,* 2015).

Z_{ML} is often used for evaluation of air quality models and atmospheric dispersion models (Davies *et al.,* 2007), as key boundary conditions for footprint models estimating the source area of observed turbulent fluxes (Kljun *et al.,* 2015), for the improvement of the inversion of surface PM concentrations from satellite-derived aerosol optical depth (Boyouk *et al.,* 2010), and, as it responds to surface energy exchange processes, it is critical for modelling climate conditions in urban settings (Onomura *et al.,* 2015).

While ML growth is linked to solar radiation, sensible heat flux (e.g. Pal and Haeffelin, 2015) and friction velocity (Batchvarova and Gryning, 1991), local circulation patterns induced by orography or land–sea contrasts generate very complex layering of the near-surface atmosphere (e.g. Boselli *et al.,* 2009). Similarly, cities can cause the ML to grow higher than over their moist rural surroundings (e.g. Barlow *et al.,* 2015). However, high PM concentrations (e.g. measured in Chinese cities) may cause the ABL to become more stable (Petäjä *et al.,* 2016), restricting ML growth which again increases near-surface PM levels. Given the diversity of urban areas across the world (e.g. geographic location, size, population density, building morphology, orography and surrounding land cover) a wide range of boundary-layer characteristics need to be quantified. While modelling studies help explore the relative importance of enhanced roughness, anthropogenic heat, the urban heat island effect (Sun *et al.,* 2016), orography, local circulation patterns, and synoptic conditions, observations to verify results remain scarce.

Automatic lidars and ceilometers (ALC) are very suitable for operation in urban areas (e.g. Wiegner *et al.,* 2006; Pandolfi *et al.,* 2013; Curci *et al.,* 2015) due to their compact design with eye-safe lasers, low cost, few maintenance requirements, high range resolution (~10 m), and their lack of noise pollution. ALC studies have examined local, synoptic- and large-scale circulation patterns such as sea-breezes, mountain-breezes, or monsoon winds which are widely recognised to affect diurnal and seasonal patterns of the boundary layer over cities (e.g. Beijing, Tang *et al.,* 2016; Marseille, Lemonsu *et al.,* 2006; Vancouver, van der Kamp and McKendry, 2010). Based on 3 years of lidar observations in Naples, Boselli *et al.* (2009) demonstrate the complex structure of the ABL when influenced by a combination of land–sea contrast and orographic effects.

Long-term studies (≥1 year) at (sub-) urban locations are increasingly available (Table 1) allowing for seasonal variations in the diurnal evolution of the urban boundary layer to be evaluated. While instrument set-up, Z_{ML}-detection method and the derived statistics (e.g. how average growth rate is defined; seasonal or monthly statistics) may differ, patterns of Z_{ML} do start to emerge (Table 1). Average daily maximum Z_{ML} usually is lowest in winter, while highest values may be reached in summer (commonly in Europe, Houston), spring (Beijing), or autumn (Shanghai, Hong Kong), depending on the seasonal variations of synoptic conditions in the study area. Coastal sites tend to have significantly lower maximum values compared to continental settings (e.g. Leipzig, Paris). For Barcelona, marine suppression of ML growth is stronger in summer, so Z_{ML} tends to be higher during colder months (Sicard *et al.,* 2006).

Average statistics and day-to-day variability of maximum Z_{ML} change with season (e.g. standard deviation in summer is greater than in winter in Paris: Pal and Haeffelin, 2015). However, the range of diurnal maxima across seasons decreases with reduced seasonality in incoming short-wave radiation towards the Equator (e.g. Shanghai, Hong Kong). Long-term studies show Z_{ML} statistics may vary inter-annually (e.g. Stachlewska *et al.,* 2012; Yang *et al.,* 2013; Zhang *et al.,* 2013; Pal and Haeffelin, 2015).

As atmospheric pollution is a major concern in London (e.g. Visser *et al.,* 2015), several campaigns have studied boundary-layer dynamics in this city based on Doppler lidar and ceilometer measurements (as part of e.g. REPARTEE: Barlow *et al.,* 2011; ACTUAL: Barlow *et al.,* 2015; Halios and Barlow, 2018; ClearfLo: Bohnenstengel *et al.,* 2015). However, no long-term analysis covering all months and several years has yet been performed. The findings of Barlow *et al.* (2011), comparing cloud-free and overcast case-studies, highlight the impact of boundary-layer clouds on ABL dynamics. Detailed analysis of Z_{ML} statistics is required to assess the implications of cloud cover and cloud type.

The objective of this work is to determine general ABL characteristics in the dense urban setting of central London using the CABAM ("Characterising the Atmospheric Boundary layer based on ALC measurements": Kotthaus and Grimmond, 2018) algorithm applied to six years of ALC measurements. Following the introduction of the study area and methods used (section 2), the general characteristics of London's urban boundary layer are derived from CABAM results (section 3). The results are analysed with respect to how cloud

TABLE 1 Long-term (≥1 year) urban ALC data studies of the atmospheric boundary layer with the method for mixed layer height Z_{ML} detection and reported statistics (average minimum Z_{ML}, average maximum Z_{ML} and average morning transition growth rate; with respective month or season: DJF: winter, MAM: spring, JJA: summer, SON: autumn). Where available (n.r.: not reported) the variability (months or seasons, i.e. DJF: winter, MAM: spring, JJA: summer, SON: autumn) is given

City	Reference	Duration [y]	Sensor	Z_{ML} detection Method	Z_{ML} Min [m agl]	Z_{ML} Max [m agl]	Growth rate [m/hr]
Beijing, China	Tang *et al.* (2016)	3	Vaisala CL31	BLview	238 (October)–351 (May)	787 (December)–1480 (May)	9–12 hr: 114 (MAM)–102 (JJA) 12–14 hr: 119 (MAM)–165 (JJA)
Granada, Spain	Granados-Muñoz *et al.* (2012)	1	Raymetrics Raman lidar	Wavelet covariance transform (WCT)	n. r.	760 (DJF)–1320 (JJA)	n. r.
Houston, Texas, USA	Haman *et al.* (2012)	1.75	Vaisala CL31	BLview + subsequent layer attribution	100–300	1100 (DJF)–2000 (JJA)	n. r.
Leipzig, Germany	Baars *et al.* (2008)	1	Polly Raman lidar	WCT and gradient method	n. r.	800 (DJF)–1800 (JJA)	100–500 (clear sky days)
London, UK	This study	6	Vaisala CL31	CABAM	134 m agl (Clear)–303 m agl (Cu)	921 (DJF)–1516 (JJA)	174
Paris, France	Pal and Haeffelin (2015)	6	Leosphere ALS-450	STRAT+	~200**	1033 (DJF)–1947 (JJA)	149 (DJF)–247 (JJA)
Shanghai, China	Peng *et al.* (2017)	1	Vaisala CL51	Idealised profile	n. r.	650 (clear JJA)–1050 (cloudy SON)	25 (MAM)–100 (SON)
Vancouver, Canada	van der Kamp and McKendry (2010)	2	Vaisala CL31	Idealised profile and gradient method	n. r.	300**(DJF)–450**(JJA)	384 (days with ABL-clouds)
Vienna, Austria	Lotteraner and Piringer (2016)	1	Vaisala CL51	BLview + fit	~280**	800 (ONDJFM)–1600 (AMJJAS)	n. r.
Yuen Long, Hong Kong	Yang *et al.* (2013)	6.5	SESI 1000 MPL	First derivative of Gaussian filter, including cloud filter	n. r.	850 (DJF)–1050 (SON)	n. r.

**Indicates values estimated from a figure.

type, cloud cover and solar angle modify seasonal and diurnal patterns. A simple but general Z_{ML}-parameterisation scheme is presented summarising the London results to facilitate future inter-city comparisons.

2 | METHODS

2.1 | Study area and data

London, United Kingdom, with an area of 1,572 km^2 and population of 8.8m in 2016 (ONS, 2017), clearly affects atmospheric conditions via the urban energy balance and emissions of pollutants (e.g. Kotthaus and Grimmond, 2014a; 2014b; Ward *et al.,* 2015; Björkegren and Grimmond, 2017). The study area is located in central London where surface roughness is high (Kent *et al.,* 2017).

The ABL is characterised using six years (2011–2016) of observations from a Vaisala CL31 ceilometer within the LUMO network (http://micromet.reading.ac.uk/). An additional year (2017) of observations is used in an independent evaluation. Initially (1 January 2011–2 March 2011) the sensor was located at KCL (51°30′42.408″N, 0°7′0.3066″W) but for the majority of the time (9 March 2011–31 December 2017) it was operated at the MR site (51°31′21.108″N, 0°9′16.4376″W) with respective sensor heights above ground-level (agl) of 32.1 m (KCL) and 4 m (MR).

For evaluation purposes, additional data are used. Cloud amount and cloud base height (CBH) of the lowest cloud layer are extracted from hourly SYNOP reports (Met Office, 2012) for 2017 and processed according to Kotthaus and Grimmond (2018). All data recording and analysis use UTC. Time stamps denote time ending of an averaging period. Data analysis is done in R (R Core Team, 2017).

2.2 | Characterisation of the atmospheric boundary layer

The CABAM algorithm (Kotthaus and Grimmond, 2018) is used to automatically track the mixed layer height and to classify the ABL into different classes based on cloud cover and cloud type. This algorithm is solely based on ALC measurements (i.e. attenuated backscatter profiles and CBH). The details of the methods are open and results perform well against independent reference observations (Kotthaus and Grimmond, 2018). The mixed layer height was evaluated against temperature inversion heights from Aircraft Meteorological Data Relay (AMDAR: Met Office, 2008) observations and the CABAM classification was compared against SYNOP reports. The latter performs especially well during daytime (Kotthaus and Grimmond, 2018). Ripple effects and near-range artefacts (Kotthaus *et al.,* 2016) lead to erroneous layers being associated with Z_{ML} at times. Hence, supervised Z_{ML} results (Kotthaus and Grimmond, 2018) are used here for analysis.

To classify ABL cloud conditions, cloud cover and cloud type are determined from the ALC measurements. This allows the methodology to be independent from auxiliary observations which may be unavailable for a study area (e.g. cloud type is unavailable for central London). The classification uses CBH reported by the ALC with the continuous 24 hr from sunset to sunset as a base period. The day centred on sunrise is hereafter indicated as day_{SR} (subscript "SR" for sunrise). This definition ensures the nocturnal period is treated as a continuous entity. For each night and following day, the ABL class is determined: Clear – predominantly clear sky, Cu – dominated by convective clouds, St - dominated by stratiform clouds, "Z_{ML} < Cu" – mixed layer height remains below CBH of convective ABL clouds, and "Z_{ML} < St" – mixed layer height remains below CBH of stratiform ABL clouds.

2.3 | General description of the ABL diurnal pattern

Several indicators are commonly used to describe the diurnal evolution of the mixed layer height: nocturnal minimum, daily maximum, morning transition (MT) growth rate, growth duration, and timing of the evening transition (ET) when turbulence breaks down. Long-term or automated studies require clear definitions of these metrics. MT onset may be defined as sunrise, the time when the surface sensible heat flux changes sign (e.g. Pal and Haeffelin, 2015), or the time of "significant" increase in growth rate, while its end is often assigned to the time when 90% of the diurnal maximum value is reached (e.g. Pal and Haeffelin, 2015).

The ET is more difficult to identify using aerosols as tracers, given that changes in atmospheric conditions are not as distinct as in the morning. Uncertainty of ALC-derived Z_{ML} is pronounced as aerosols may remain dispersed within the ABL even if turbulent mixing is reduced. This leads to the emerging residual layer often associated with Z_{ML} (Haeffelin *et al.,* 2012; Peng *et al.,* 2017). Atmospheric stability (e.g. measured via lapse rates or eddy covariance) can help identify transitions of the nocturnal (often stable) layer into the convective daytime boundary layer during MT and back to the nocturnal stratification during ET (e.g. Pal and Haeffelin, 2015).

Given that the objective of the current work is to only require ALC observations, general indicators are defined using these and significant solar positions (Table 2).

3 | RESULTS

3.1 | Classification

ABL conditions in central London for the study period (2011–2016) are classified based on ALC observations using the CABAM algorithm (Kotthaus and Grimmond, 2018). Of the total possible SR-centred 24 hr periods (number of

TABLE 2 General indicators used to describe the diurnal evolution of the mixed layer height Z_{ML} in this study. Significant solar positions are marked by sunrise (SR), solar noon (SN), sunset (SS), and midnight (MN); MT and ET are the morning and evening transition, respectively. Thresholds for the definition of MT are chosen in accordance with median diurnal patterns of MT growth rate (Figure S2, Supporting Information).

Time	Height	Description	Definition
t_{min}	z_{min}	minimum Z_{ML}	between SS and SN
t_{max}	z_{max}	maximum Z_{ML}	between t_{min} and SS
	z_{eve}	minimum evening Z_{ML}	between SN and MN
$t1_{MT}$	$z1_{MT}$	MT onset	$Z_{ML} \geq z_{min} + 0.1 \times (z_{max} - z_{min})$ for the first time after SR
$t2_{MT}$	$z2_{MT}$	MT end	$Z_{ML} \leq z_{min} + 0.8 \times (z_{max} - z_{min})$ for the last time before t_{max}
$t1_{ET}$	$z1_{ET}$	ET onset	$Z_{ML} \leq z_{max} - 0.2 \times (z_{max} - z_{eve})$ for the first time after t_{max}
$t2_{ET}$	$z2_{ET}$	ET end	$Z_{ML} \geq z_{max} - 0.8 \times (z_{max} - z_{eve})$ for the last time after $t1_{ET}$
	Δz_{MT}	MT dilution height	$z2_{MT} - zt1_{MT}$
	Δz_{noc}	Nocturnal decay	$z2_{ET} - z_{min}$
Δt_{MT}		MT duration	$t2_{MT} - t1_{MT}$
Δt_{noc}		Nocturnal decay duration	$t2_{ET} - t_{min}$
	GR_{MT}	MT growth rate	$\Delta t_{MT}\ \Delta t_{MT}^{-1}$
	DR_{noc}	Nocturnal decay rate	$\Delta z_{noc}\ \Delta t_{noc}^{-1}$

$day_{SR} = 2192$), 5% could not be classified because of insufficient data and 8% are classified as rainy (i.e. complex rain patterns with a duration of >4 hr impede the successful tracing of Z_{ML}). Another 12% experience >2 hr of precipitation with no major impact on Z_{ML}-detection so they are merged with their respective cloud class for the analysis presented.

The frequency distribution of ABL classes (Table 3) shows convective clouds clearly dominate London's boundary layer during daytime (Cu: 60%, Z_{ML} < Cu: 5%), with 12% considered cloud free, and 22% are dominated by stratiform clouds at the top of the mixed layer. During night, all categories apart from Z_{ML} < St show a similar frequency between 20 and 31%, with clear nights being most likely. It should be noted that the conditions for a night to be classified as Clear are more relaxed than during daytime, i.e. some of the Clear nights may have a cloud layer above the ML. The mixed layer is "cloud-topped" if Z_{ML} is located near the reported CBH. The CABAM classification scheme performs better during daytime when compared to SYNOP reports (Kotthaus and Grimmond, 2018).

While both Clear (79%) and St (54%) nights are most likely to follow a night of the same class, the Cu category is less persistent with similar chances for a Cu day to be detected after a night classified as Clear (28%), Cu (28%) or Z_{ML} < Cu (24%). Days with the mixed layer remaining below CBH most often follow a clear or Z_{ML} < CBH night.

Classes with similar diurnal and seasonal evolution (not shown) are combined to increase the number of samples for statistical analysis (sections 3.2, 3.3), i.e. for days with Cu, the nocturnal classes of Z_{ML} < Cu and Clear are merged, all classes with Z_{ML} < CBH during day are combined, and the

TABLE 3 Occurrence of ABL classes (Clear, Cu, St, Z_{ML} < Cu and Z_{ML} < St) in central London derived using the CABAM algorithm (Kotthaus and Grimmond, 2018) for the study period 2011–2016. Columns (rows) indicate daytime (night-time) categories given as (a) total number of 24 hr periods (no. of day_{SR}), (b) percentage of total number of periods (last column) classified into the respective category during night (f_{night} [%]), (c) percentage of total number of periods (last row) classified into the respective category during day (f_{day} [%]), and (d) percentage of total number of periods classified (f_{total} [%]). day_{SR}-periods (166) with precipitation impeding the detection of Z_{ML} are excluded; classes indicating little rain or fog are merged into the respective cloud class

(a) no.of day_{SR}
(b) f_{night} [%]
(c) f_{day} [%]
(d) f_{total} [%]

Night \ Day	Clear		Cu		St		Z_{ML} < Cu		Z_{ML} < St		Total
Clear	**187**	31	321	54	30	5	54	9	4	1	596
	79	10	28	17	7	2	56	3	40	0	31
Cu	22	5	**316**	71	97	22	10	2	2	0	447
	9	1	28	16	23	5	10	1	20	0	23
St	9	2	209	46	**230**	51	3	1	0	0	451
	4	0	18	11	54	12	3	0	0	0	24
Z_{ML} < Cu	18	5	278	73	53	14	**27**	7	3	1	379
	8	1	24	15	13	3	28	1	30	0	20
Z_{ML} < St	2	5	25	57	13	30	3	7	**1**	**2**	44
	1	0	2	1	3	1	3	0	10	0	2
total	238	12	1149	60	423	22	97	5	10	1	**1917**

two nocturnal cloud classes are combined for both the daytime Cu and St class, respectively. This leaves five major ABL classes to be analysed: Clear – predominantly clear, Cu – dominated by convective clouds, St – dominated by stratiform clouds, ClearCu – predominantly clear night followed by a day with convective clouds, and "$Z_{ML} < CBH$" – mixed layer height remains below CBH of ABL clouds during daytime.

The frequency of these major ABL classes by season (Figure 1) reveals more periods are excluded due to rainfall in the summer compared to colder seasons as cloud patterns are more complex and inhibit successful Z_{ML} detection. The likelihood for St is 4.5 times greater in winter than summer, while the seasonal variability for the Cu class is much smaller. Clear nights in summer are ~2.5 times more likely to be followed by a day with convective clouds (ClearCu) than in winter. Completely clear days are most frequent in spring, while the generally rare $Z_{ML} < CBH$ class is least frequent in autumn. These results are similar to those obtained from SYNOP reports for the Greater London area (Kotthaus and Grimmond, 2018) which indicate St is 3.7 times more frequent in winter than summer and which confirm low seasonality of Cu. From SYNOPS, both the Clear and ClearCu classes are most likely in spring.

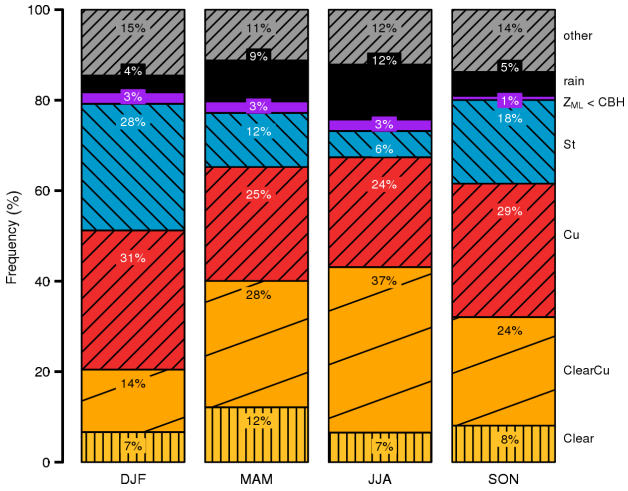

FIGURE 1 Relative frequency of major ABL classes (see text for definitions) in central London, UK, by season, including days when complex rain patterns obstructed the detection of mixed layer height ("rain"). Classification for the study period (2011–2016) derived using the CABAM algorithm (Kotthaus and Grimmond, 2018) with ALC observations [Colour figure can be viewed at wileyonlinelibrary.com].

3.2 | Seasonal–diurnal patterns

Median diurnal patterns of Z_{ML} are calculated by season and major ABL class (section 3.1) for the 24 hr periods centred at sunrise (day_{SR}). Data availability (Figure 2, line plots) for each 15 min interval is shown as a percentage of the total number of days (no. of day_{SR}) within the category (i.e. for a class occurring with the same frequency in all seasons, the maximum possible availability is 25%). Excluding the "rain" class (section 2.2), data availability (Figure 2f) peaks between 22.3% (summer) and 24.8% (winter) and is rather consistent throughout the day for all classes (apart from near sunset with the seasonal changes in solar angle). Z_{ML} of all classes and seasons (Figure 2) generally have the expected diurnal evolution with a minimum around sunrise and peak values in the afternoon. Overall, seasonal variations are distinct and diurnal patterns clearly depend on ABL class.

Under Clear conditions (Figure 2a), nocturnal Z_{ML} varies with season with lowest values in winter and autumn (25^{th} percentile ~130 m agl) and highest in summer. In all seasons, growth starts several hours after sunrise. Daytime evolution is very similar in spring and autumn, with values levelling off after solar noon only slightly lower than in summer (1200–1400 m agl), while the maximum of the median cycle is only 719 m in winter.

When convective clouds are present on the day following a clear night (Figure 2b), higher afternoon Z_{ML} occur in most seasons compared to clear days (Figure 2a). Only in autumn does growth level off shortly after solar noon in the cloudy case (Figure 2b). As growth continues under clear conditions (Figure 2a), the maximum values reached are similar. Afternoon Z_{ML} does not differ much between spring and summer for ClearCu conditions. Before sunrise, spring, summer and autumn all have the same seasonal relation as found for the Clear ABL class. However, in winter the detected mixed layer starts to grow earlier so that median values around sunrise are highest in the cold season. This is explained by CBH of convective clouds near sunrise being higher in winter (Figure S1, Supporting Information) and a higher fraction (28% compared to 17% in summer) of Z_{ML} in the 4 hr around SR being associated with clouds.

Under Cu conditions (Figure 2c), the median nocturnal Z_{ML} in winter differs from those observed in the other seasons, again due to seasonality in CBH (Figure S1, Supporting Information). While Z_{ML} exhibits a slight decrease in the time from sunset to sunrise for the other seasons, nocturnal decay is less pronounced in winter with rather stable median values in the time before SR. Overall, nocturnal values are higher for Cu (Figure 2c) compared to Clear nights (Figure 2a,b) leading to reduced growth rates in the cloudy class. It appears that CBH and associated Z_{ML} are slightly lower on days with convective clouds following a cloudy night (Figure 2c) compared to ClearCu (Figure 2b) conditions.

As expected, the amplitude of the diurnal cycle is least when stratiform clouds (Figure 2d) occur, with minimal seasonal differences. As the "$Z_{ML} < CBH$" class is rare in all seasons (Figure 2), median patterns are noisy compared to other classes (Figure 2e). The nocturnal values are similar to clear nights (i.e. low). Daytime values remain lower than for Clear (Figure 2a) or convective cloud (Figure 2b,c) classes.

Across all classes (Figure 2f), Z_{ML} is highest in summer throughout day and night compared to spring and autumn.

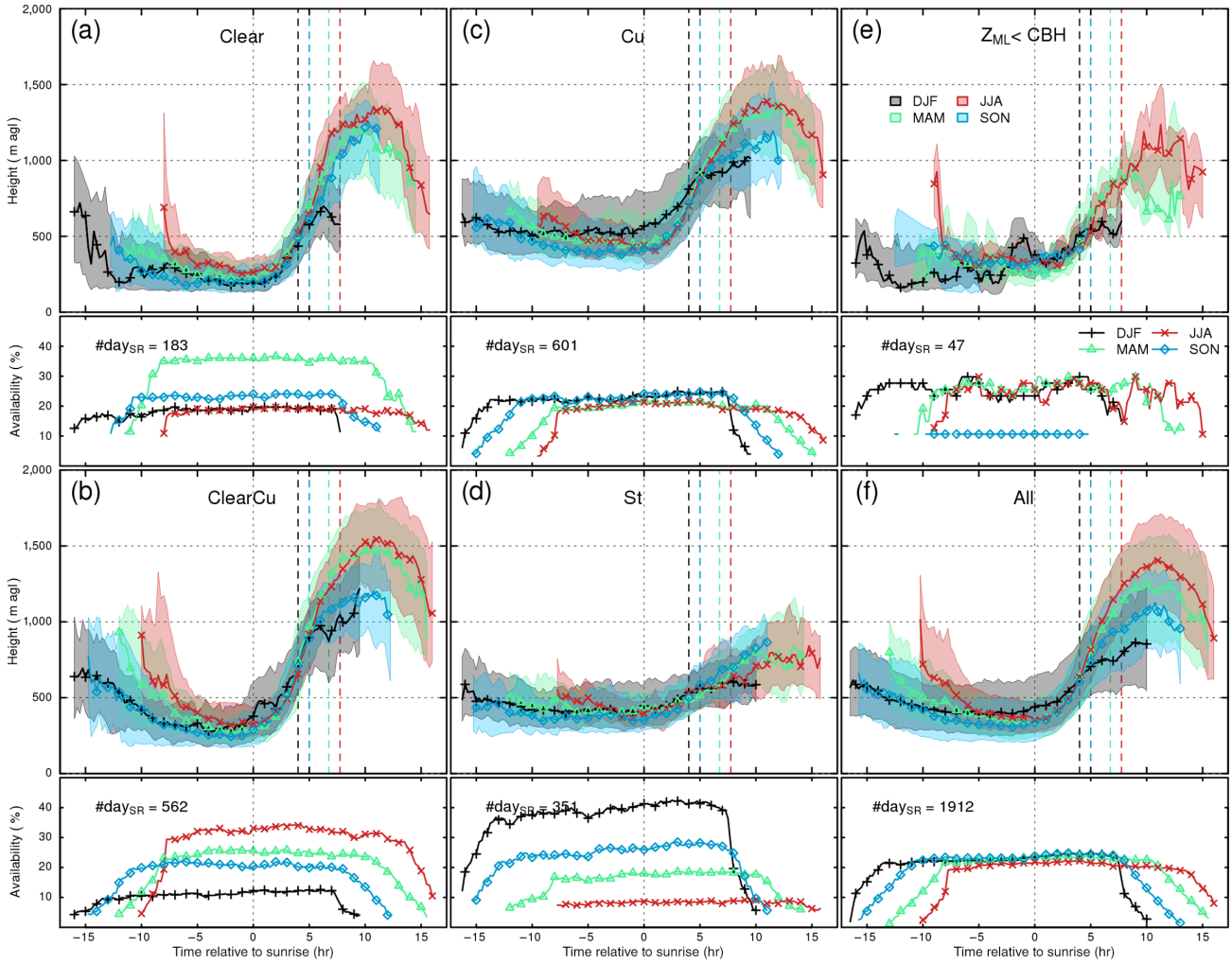

FIGURE 2 Median seasonal diurnal patters relative to sunrise of mixed layer height Z_{ML} in central London, UK, for 2011–2016. The CABAM algorithm (Kotthaus and Grimmond, 2018) is used to detect Z_{ML} and classify 24 hr periods centred around sunrise (day_{SR}) based on ABL characteristics. Major classes are (a) Clear, (b) Clear night followed by day with convective clouds (Cu), (c) Cu, (d) stratiform clouds (St), and (e) Z_{ML} below cloud base height (CBH), with (f) all combined. (a, c, e): (solid line) median and (shading) inter-quartile range, (b, d, f): occurrence as percentage of total number of days within the category (no. of day_{SR}). Periods with (a, b, c, d, f) < 20 or (e) <5 samples are excluded. Vertical dashed lines indicate the seasonal average time of solar noon [Colour figure can be viewed at wileyonlinelibrary.com].

In winter, Z_{ML} decreases less through the long nights so that median values of Z_{ML} at sunrise are higher than in all other seasons. The low growth rates and short day-length still result in winter afternoon Z_{ML} being the lowest. This analysis of seasonal diurnal patterns (Figure 2) demonstrates the importance of boundary-layer clouds to the interpretation of Z_{ML} in areas such as the United Kingdom, where both convective and stratiform clouds often affect ABL dynamics.

3.3 | Generalised ABL characteristics

To quantify ABL characteristics in central London, several indicators related to diurnal Z_{ML}-evolution (section 2.3, Table 2) are calculated for each day_{SR} by season and ABL class (Figure 3). As expected from the analysis of median diurnal patterns (section 3.2), many indicators show distinct seasonal variations.

Nocturnal Z_{ML} tends to decrease slightly (Figure 3s), especially under clear-sky conditions in spring and summer with median $\Delta z_{night} = 33$ m/hr. Winter nights and those associated with stratiform clouds show less height variation. When considering all ABL classes, the time of minimum Z_{ML} (Figure 3k) varies through the night. The overall median t_{min} is at $0.72 \times H_{night}$. Minima occur slightly later in the warmer seasons compared to winter and autumn, and slightly earlier for clear nights compared to cloudy cases, e.g. median t_{min} in summer is $0.75 \times H_{night}$ for Clear and $0.98 \times H_{night}$ for St. Minimum Z_{ML} observed in central London (Figure 3o) strongly depends on the ABL class. Median z_{min} ranges between 134 m agl (Clear) and 303 m agl (Cu). Seasonal differences within the same class are smaller than inter-class variations, e.g. for the Clear class median z_{min} is between 128 m agl (DJF and SON) and 181 m agl (JJA). These heights are a little lower than reported for Vienna and Paris (Table 1). Beyond location, land use and synoptic conditions, the lower values reported for London may be due to a reduced bias to higher layers being detected with the current approach, given values as low as 50 m are detectable (Kotthaus and Grimmond, 2018).

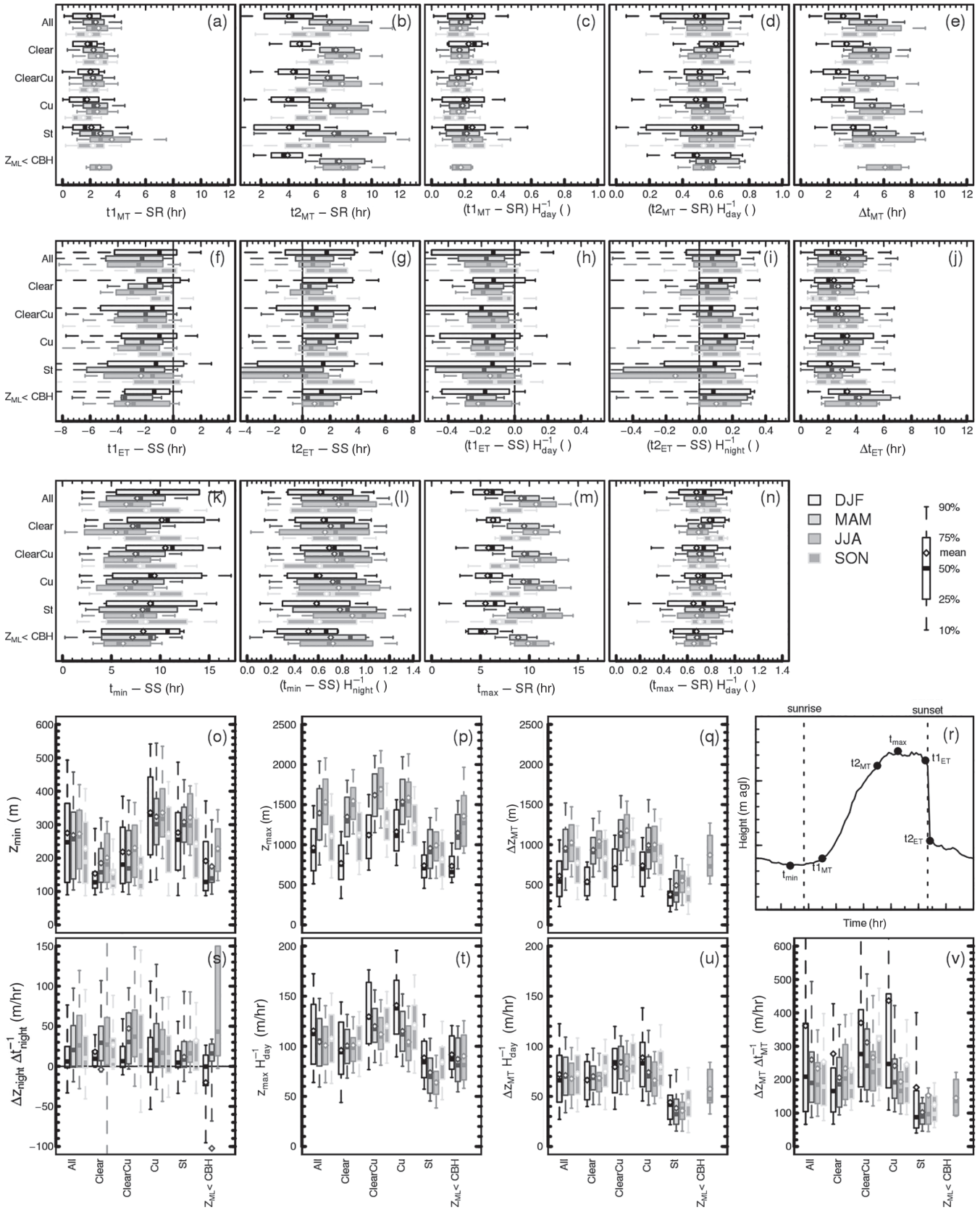

FIGURE 3 General indicators' statistics of the diurnal evolution (sketch in subplot (r)) of the mixed layer height Z_{ML} in central London detected by the CABAM algorithm (Kotthaus and Grimmond, 2018) using ALC measurements (2011–2016). Results are grouped by major ABL class (Clear, ClearCu, Cu, St, $Z_{ML} < CBH$, and All combined; section 3.1) and season. See section 2.3 and Table 2 for symbol definitions. To account for impact of changes in daylight hours (H_{day}), (a) $t1_{MT}$, (b) $t2_{MT}$, (m) t_{max}, (p) z_{max}, and (q) Δz_{MT} are displayed also (c,d,n,t,u) normalised by day-length; (f) $t1_{ET}$, (g) $t2_{ET}$, and (k) t_{min} are (h,i,l) divided by night-length ($H_{night} = 24 - H_{day}$). Temporal indicators are given in time relative to sunrise (SR) or sunset (SS), respectively

While long-term eddy covariance (Wood *et al.,* 2010) and scintillometry (Crawford *et al.,* 2016) observations in central London suggest a likelihood of 20–40% for the nocturnal mixed layer to remain < 200 m, CABAM detects Z_{ML} < 200 m for 13% (between SS + 1 hr and SR). For another 5% of this time, no Z_{ML} is found but at least one higher layer (representing e.g. the residual layer) is identified suggesting the algorithm considers the possibility that Z_{ML} might be located below the detection limit of 50 m or measurement noise prevents successful tracking of Z_{ML} at heights below 100 m. While this indicates general consistency between CABAM-derived Z_{ML} and tower-based observations, direct comparison should be performed to assess conditions that might cause disagreement between the approaches.

z_{max} clearly varies with both ABL class and season (Figure 3p). The latter effect is partly explained by the prolonged growth duration (Figure 3e) in spring and summer, as the maximum is reached much later in the day (Figure 3m) with median t_{max} converging around $0.74 \times H_{day}$ (Figure 3n). Consistently, statistics of z_{max} become more similar (∼105 m/hr) when normalised by H_{day} (Figure 3t), especially for the Clear class. However, for cloudy daytime conditions additional factors must play a role as the seasonal variation is reversed after normalisation (cf. Figure 3p,t). With all classes combined, z_{max} in summer (winter) is 1516 m agl (921 m agl). Lowest median z_{max} is detected during winter St conditions (707 m agl) and highest during summer ClearCu (1704 m agl). For the class Z_{ML} < CBH, median normalised z_{max} (82 m/hr) is lower compared to Clear conditions (100 m/hr). This London z_{max} is similar to that observed in Leipzig and Vienna, but slightly lower than in Paris and Houston (Table 1).

Start and end of the MT define the period of most significant increase in Z_{ML}. While MT starts on average ∼2 hr after sunrise (Figure 3a,c), the end of MT is clearly a function of day-length (Figure 3b,d). The inter-quartile range (IQR) is highest for the St class due to the increased uncertainty in detecting ABL indicators associated with the shallow diurnal amplitude (Figure 2d). On average, MT spans from $0.17 \times H_{day}$ to $0.62 \times H_{day}$ and lasts (Figure 3e) 3.5 hr (6.75 hr) in winter (summer). Baars *et al.* (2008) note that very short MT duration is often linked to extremely high growth rates.

The MT dilution height Δz_{MT} (Figure 3q) here represents the increment of Z_{ML} during MT (Table 2) and ∼80% of the daily amplitude ($z_{max} - z_{min}$). When normalised by H_{day} (Figure 3u), Δz_{MT} is very consistent within ABL classes, with median values ranging from 42 m/hr (St) to 62 m/hr (ClearCu). The MT growth rate (Figure 3v) is not normally distributed (mean > median), which is consistent with statistics reported elsewhere (e.g. Pal and Haeffelin, 2015). Median growth rate for the Clear class is identical with the overall average of 174 m/hr, which is only slightly stronger than for Cu (169 m/hr). Growth rate is strongest (weakest) for the ABL class ClearCu (St) with 212 m/hr (92 m/hr) and in-between for Z_{ML} < CBH (134 m/hr). This is consistent with findings for Paris (Pal *et al.,* 2013) where enhanced growth rates were also found on days when cumulus clouds form at the top of the mixed layer during daytime, compared to completely clear-sky conditions. However, growth rates in London are generally slightly weaker than in Paris (Pal and Haeffelin, 2015).

For London, seasonal variations in growth rate are negligible compared to inter-class differences (Figure 3v). Other urban studies (Table 1) suggest MT growth to be stronger in spring (e.g. Magurele (Romania): Sokół *et al.,* 2014) or summer (e.g. Paris: Pal and Haeffelin, 2015) when energy fluxes of radiation and sensible heat flux peak.

Compared to the MT statistics, greater overall variability (IQR) is found in the temporal indicators of ET (Figure 3f,g). Seasonal variations are of similar magnitude for beginning ($t1_{ET}$) and end ($t2_{ET}$) of this transition, so that the overall duration Δt_{ET} (Figure 3j) consistently varies around the median value of 2.5 hr.

Overall median statistics are consistent with other European studies. However, care should be taken when directly comparing Z_{ML} indicators reported for different cities, given the variety of methods used. Not only do the studies differ in terms of instrumentation and Z_{ML}-detection algorithm (Table 1); also, a range of definitions are applied to determine the significant indicators. Most notably, MT onset (here $t1_{MT}$) is identified based on a range of criteria, including sunrise, time of increasing growth rate, time of Z_{ML} reaching a certain increment compared to z_{min}, and time of cross-over of the surface sensible heat flux from negative to positive values. The definition of this point clearly affects derived statistics of growth rate and MT duration. Given that reports on ET indicators are still rare, no common definition for its indicators is available yet.

The statistical analysis (Figure 3) suggests that for central London, a substantial proportion of seasonal variability in indicators that describe the diurnal pattern of Z_{ML} is related to variations in daylight hours; while the behaviour of MT and ET mostly depends on solar position, minimum and maximum Z_{ML} as well as MT growth rate are clearly also a function of ABL class.

3.4 | ABL parameterisation

General Z_{ML} characteristics of London's urban boundary layer are extracted based on the statistical analysis (section 3.3) of long-term observations by season and ABL class and used to compile a simple, first-order parameterisation of the Z_{ML} diurnal cycle solely based on ABL class and day-length. While temporal indicators are expressed relative to day-length, heights are estimated as a function of three ABL-class dependent parameters, namely z_{min}, MT growth rate (GR_{MT}), and nocturnal decay rate (DR_{noc}; Table 4). Representative GR_{MT} and DR_{noc} estimates are the overall median

TABLE 4 (a) Parameterisation for indicators describing average mixed layer height over London as a function of day length H_{day} ($H_{night} = 24 - H_{day}$), sunrise (SR), sunset (SS) and ABL class-specific coefficients: (b) z_{min}, GR_{MT}, and DR_{noc} (Table 2). Empirical coefficients are derived from statistical analysis (section 3.3)

(a)		(b)			
Indicator	**Parameterisation**	**Class**	**z_{min} [m agl]**	**GR_{MT} [m/hr]**	**DR_{noc} [m/hr]**
t_{min}	$(SS-24) + 0.72 \times H_{night}$	All	338	187	1.28
$t1_{MT}$	$0.17 \times H_{day} + SR$	Clear	218	182	1.66
$t2_{MT}$	$0.53 \times H_{day} + SR$	ClearCu	281	229	2.16
t_{max}	$0.74 \times H_{day} + SR$	Cu	397	186	1.17
$t1_{ET}$	$-0.15 \times H_{day} + SS$	St	340	91	0.59
$t2_{ET}$	$0.01 \times H_{night} + SS$	$Z_{ML} < CBH$	277	140	1.19
$z1_{MT}$	$z_{min} + 0.1 \times GR_{MT} \times (t2_{MT} - t1_{MT})$				
$z2_{MT}$	$z_{min} + 0.8 \times GR_{MT} \times (t2_{MT} - t1_{MT})$				
z_{max}	$z_{min} + GR_{MT} \times (t2_{MT} - t1_{MT})$				
$z2_{ET}$	$z_{min} + DR_{noc} \times H_{day} \times H_{night}$				
$z1_{ET}$	$z_{max} - 0.2 \times (z_{max} - z2_{ET})$				

values by class, while the 75th percentile of z_{min} is found most appropriate.

Using examples for the winter and summer solstice, results from this empirical model are determined for the range of possible daylight hours at the study site (Figure 4a,b), exemplary for all ABL classes combined (All), St and ClearCu. Comparison to observed median diurnal patterns for the three months around the solstice dates shows the first-order parameterisation is capable of reproducing seasonal dependence and general behaviour for the major ABL classes. As expected, morning and evening transition periods are the most challenging times to describe. Further studies are required to gain a better understanding of these transition times.

To qualitatively assess the ability of the proposed parameterisation to describe the ABL structure, an independent year (2017) is analysed. The ABL classes (Clear, ClearCu, Cu, and St) determined from SYNOP observations (Kotthaus and Grimmond, 2018) are used with the empirical model (Table 4) to obtain the diurnal evolution of Z_{ML}. These results are compared to median supervised Z_{ML} observations (Figure 4c–f) for those days.

Using only the commonly available SYNOP observations, the parameterisation results show generally good agreement with the average ABL patterns observed for the different categories (Figure 4c–f). Some uncertainty is introduced considering Greater London SYNOP reports might not fully represent the central urban study area (Kotthaus and Grimmond, 2018). The simple model is not designed to resolve day-to-day variability of the ABL structure within a category for comparable sun-angles. However, interannual variations (e.g. Pal and Haeffelin, 2015) might explain some of the discrepancies such as the tendency for underestimation of Z_{ML} during Cu days (Figure 4e) or the premature rise during mornings with St cloud cover (Figure 4f). Future studies covering a range of time periods and additional study areas will be conducted to further evaluate the general applicability of this simple model.

4 | SUMMARY AND DISCUSSION

The CABAM (Characterising the Atmospheric Boundary layer (ABL) based on automatic lidar and ceilometer (ALC) Measurements) algorithm (Kotthaus and Grimmond, 2018) is used with ALC data to automatically track the mixed layer height Z_{ML} and to classify ABL characteristics with respect to cloud cover and cloud type. Classes distinguish nights and days affected by clear sky (Clear), convective clouds (Cu), stratiform clouds (St), or Z_{ML} remaining below cloud base height (CBH) of boundary-layer clouds.

CABAM is applied to characterise ABL conditions for central London, United Kingdom, for a multi-year period (2011–2016) based on observations of a Vaisala CL31 ceilometer. Excluding days when complex rain patterns prevent tracking of Z_{ML}, five major ABL classes occur: (a) Clear, (b) Cu, (c) St, (d) clear night followed by day with convective clouds (ClearCu), and (e) days with $Z_{ML} < CBH$. While convective clouds generally dominate, the relative frequency of the major ABL classes varies with season. Cu always makes up ~30%, while the likelihood for St is 4.5 times greater in winter than summer. Clear nights are ~2.5 times more likely to be followed by a day with convective clouds (ClearCu) in summer than winter. Completely clear days are most frequent in spring. The rare "$Z_{ML} < CBH$" class is least likely in autumn. These findings are generally in agreement with SYNOP reports again omitting days with complex rain patterns.

From this dataset, median statistics for critical points in the diurnal evolution of the mixed layer (minimum, morning transition, maximum, evening transition) are determined. Two aspects clearly shape the diurnal evolution of Z_{ML} over London: (a) day-length and (b) ABL category related to cloud

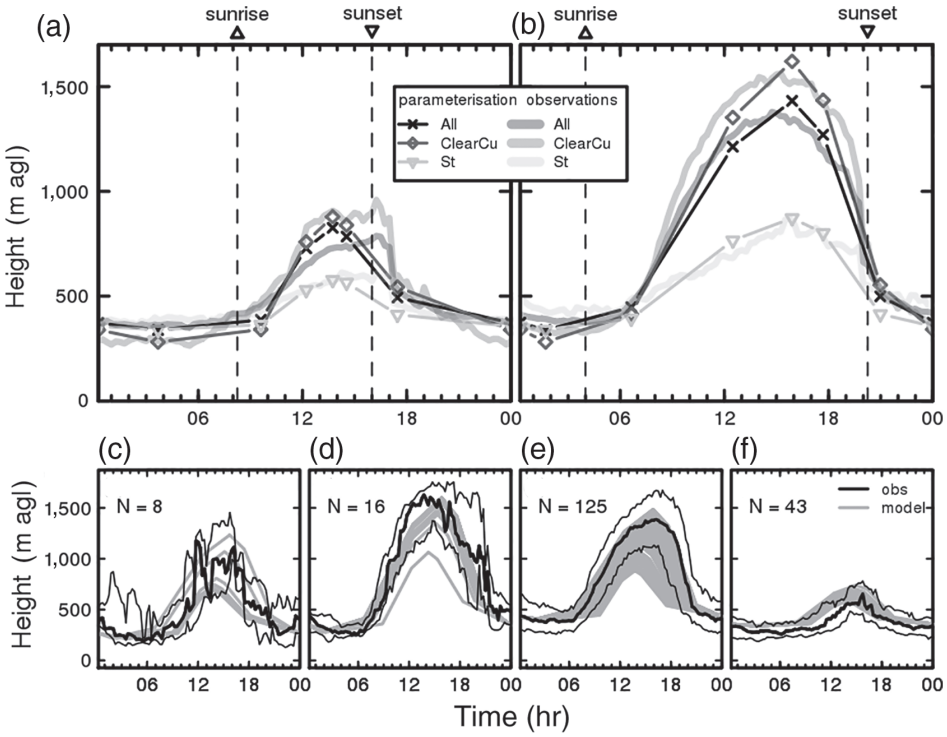

FIGURE 4 Results from a simple empirical model (Table 4) to describe mixed layer height Z_{ML} in central London as a function of selected ABL class determined from (a, b) ALC in 2011–2016 and (c–f) SYNOP reports in 2017: (a) for ClearCu, St and All combined (lines with symbols) model results for winter solstice with (thick lines) median diurnal patterns observed in the three months around this date between 2011 and 2016, (b) same as (a) for summer solstice, (c–f) individual model results (coloured lines) for days classified as (c) Clear, (d) ClearCu, (e) Cu and (f) St, respectively, in 2017 with (thick lines) median diurnal pattern observed for these days and (thin black lines) inter-quartile range. (c–f) Number of days N in 2017 within each class

cover and cloud type. With all data combined, the median daytime maximum is clearly lower in winter (921 m agl) than in summer (1516 m agl). A dependence on ABL class is detected. The median morning transition growth rate ranges from 92 m/hr (St) to 212 m/hr (ClearCu), with an overall average of 174 m/hr. These differences by ABL class clearly translate into the overall statistics of Z_{ML} by season due to the seasonal variations in cloud characteristics. In general, these indicators are similar to values reported for other European cities.

Where clouds of various types frequently affect the ABL, such as in the United Kingdom, general mixed layer height characteristics may vary distinctly depending on the frequency of cloud types present in the sample analysed. While observational ABL studies often apply a cloud cover filter, cloud type is usually neglected. The findings presented here clearly demonstrate the importance of cloud cover, cloud type and cloud base height for the sound interpretation of mixed layer height measurements, as suggested in previous studies (e.g. Schween *et al.,* 2014; Pal and Haeffelin, 2015). Especially stratiform clouds should be interpreted separately, as the ALC-derived mixed layer height likely coincides with the CBH rather than the actual mixed layer height due to strong attenuation of the lidar signal in such clouds.

To facilitate inter-city comparison in future studies, a simple, first-order parameterisation is proposed to describe seasonal and diurnal variations of Z_{ML} based on only ABL class and daylight hours. Three class-dependent parameters (minimum Z_{ML}, morning transition growth rate, and nocturnal decay rate) are required to determine the general evolution of Z_{ML} as a function of solar geometry (i.e. time of day, day in year) only. Comparison between this simple model and median diurnal patterns for the examples of summer and winter solstice shows overall patterns are well-described. Further, the model enables first-order prediction of Z_{ML} diurnal evolution if information on cloud type is available (e.g. from SYNOP reports). The parameterisation is considered to provide valuable insights for studies addressing the dependence of air quality on mixed layer height dynamics under different cloud conditions.

Due to limitations of the methods used, many observational studies of mixed layer height development focus on daytime conditions or do not report nocturnal statistics. Omitting the nocturnal boundary layer might increase the uncertainty in estimating the onset time of the morning transition (if determined based on Z_{ML}) and complicates the interpretation of Z_{ML} in the afternoon and evening transition when turbulent mixing decays.

While most studies focus on the morning growth period, this is one of the first studies to also address the evening transition. At this central London site a new aerosol layer usually starts forming near the surface after sunset which helps detect the end of the evening transition. Application of the CABAM

algorithm on ALC observations with complete overlap at low ranges (such as the CL31) at a rural, low-polluted site could identify if the formation of the nocturnal layer is also detectable where aerosol emission at the surface is less significant compared to the dense city centre. Results presented here for central London show the timing of the evening transition is less clearly defined than in the morning. A common definition of indicators to characterise the evening transition is critical.

While number of daylight hours, a first-order proxy for incoming short-wave radiation, explains much of the seasonal variability, other physical drivers such as anthropogenic heat emissions, sensible heat flux and atmospheric stability likely play a role (e.g. Pal and Haeffelin, 2015). Links between these processes and ABL dynamics will be evaluated in future studies using turbulent heat flux measurements and weather station observations available at different heights in central London (e.g. Kotthaus and Grimmond, 2014a; Crawford *et al.,* 2016). Definition of the critical points within the diurnal cycle of the mixed layer could be refined with interpretation of these physical drivers. The results from this study will be valuable for examining the relation between mixed layer height and atmospheric pollution concentrations in central London.

ACKNOWLEDGEMENTS

This study and ceilometer observations have received financial support from EU FP7 BRIDGE, H2020 URBANFLUXES, NERC ClearfLo NE/H003231/1, NERC APHH China AirPro NE/N00/00X/1, Newton Fund/ Met Office CSSP- China, EU COST Action TOPROF, KCL and University of Reading. KCL and ERG/LAQN are acknowledged for providing site access. We thank Charley Stockdale, Lucia Monti, Duick Young, Chris Castillo, Kjell zum Berge, Will Morrison, Elliott Warren, Lukas Pauscher, Paul Smith, Tom Smith and all other staff and students at KCL and University of Reading who are involved in the LUMO measurement network. We also thank Max Priestman and David Green at ERG for supporting the ceilometer operation. We thank the reviewers for their constructive comments.

ORCID

Simone Kotthaus http://orcid.org/0000-0002-4051-0705
C. Sue B. Grimmond http://orcid.org/0000-0002-3166-9415

REFERENCES

Baars, H., Ansmann, A., Engelmann, R. and Althausen, D. (2008) Continuous monitoring of the boundary-layer top with lidar. *Atmospheric Chemistry and Physics*, 8, 7281–7296. https://doi.org/10.5194/acp-8-7281-2008.

Barlow, J.F., Dunbar, T.M., Nemitz, E.G., Wood, C.R., Gallagher, M.W., Davies, F., O'Connor, E. and Harrison, R.M. (2011) Boundary layer dynamics over London, UK, as observed using Doppler lidar during REPARTEE-II. *Atmospheric Chemistry and Physics*, 11, 2111–2125. https://doi.org/10.5194/acp-11-2111-2011.

Barlow, J.F., Halios, C.H., Lane, S.E. and Wood, C.R. (2015) Observations of urban boundary layer structure during a strong urban heat island event. *Environmental Fluid Mechanics*, 15(2), 373–398. https://doi.org/10.1007/s10652-014-9335-6.

Batchvarova, E. and Gryning, S.-E. (1991) Applied model for the growth of the daytime mixed layer. *Boundary-Layer Meteorology*, 56, 261–274. https://doi.org/10.1007/BF00120423.

Bjorkegren, A. and Grimmond, C.S.B. (2017) Net carbon dioxide emissions from central London. *Urban Climate*, 23, 131–158. https://doi.org/10.1016/J.UCLIM.2016.10.002.

Bohnenstengel, S.I., Belcher, S.E., Aiken, A., Allan, J.D., Allen, G., Bacak, A., Bannan, T.J., Barlow, J.F., Beddows, D.C.S., Bloss, W.J., Booth, A.M., Chemel, C., Coceal, O., Di Marco, C.F., Dubey, M.K., Faloon, K.H., Fleming, Z.L., Furger, M., Gietl, J.K., Graves, R.R., Green, D.C., Grimmond, C.S.B., Halios, C.H., Hamilton, J.F., Harrison, R.M., Heal, M.R., Heard, D.E., Helfter, C., Herndon, S.C., Holmes, R.E., Hopkins, J.R., Jones, A.M., Kelly, F.J., Kotthaus, S., Langford, B., Lee, J.D., Leigh, R.J., Lewis, A.C., Lidster, R.T., Lopez-Hilfiker, F.D., McQuaid, J.B., Mohr, C., Monks, P.S., Nemitz, E., Ng, N.L., Percival, C.J., Prévôt, A.S.H., Ricketts, H.M.A., Sokhi, R., Stone, D., Thornton, J.A., Tremper, A.H., Valach, A.C., Visser, S., Whalley, L.K., Williams, L.R., Xu, L., Young, D.E. and Zotter, P. (2015) Meteorology, air quality, and health in London: the ClearfLo project. *Bulletin of the American Meteorological Society*, 96, 779–804. https://doi.org/10.1175/BAMS-D-12-00245.1.

Boselli, A., Armenante, M., D'Avino, L., D'Isidoro, M., Pisani, G., Spinelli, N. and Wang, X. (2009) Atmospheric aerosol characterization over Naples during 2000–2003 EARLINET project: planetary boundary-layer evolution and layering. *Boundary-Layer Meteorology*, 132, 151–165. https://doi.org/10.1007/s10546-009-9382-6.

Boyouk, N., Léon, J.-F., Delbarre, H., Podvin, T. and Deroo, C. (2010) Impact of the mixing boundary layer on the relationship between PM2.5 and aerosol optical thickness. *Atmospheric Environment*, 44, 271–277. https://doi.org/10.1016/j.atmosenv.2009.06.053.

Crawford, B., Grimmond, C.S.B., Ward, H.C., Morrison, W. and Kotthaus, S. (2016) Spatial and temporal patterns of surface–atmosphere energy exchange in a dense urban environment using scintillometry. *Quarterly Journal of the Royal Meteorological Society*, 143, 817–833. https://doi.org/10.1002/qj.2967.

Curci, G., Ferrero, L., Tuccella, P., Barnaba, F., Angelini, F., Bolzacchini, E., Carbone, C., Denier van der Gon, H.A.C., Facchini, M.C., Gobbi, G.P., Kuenen, J.P.P., Landi, T.C., Perrino, C., Perrone, M.G., Sangiorgi, G. and Stocchi, P. (2015) How much is particulate matter near the ground influenced by upper-level processes within and above the PBL? A summertime case study in Milan (Italy) evidences the distinctive role of nitrate. *Atmospheric Chemistry and Physics*, 15, 2629–2649. https://doi.org/10.5194/acp-15-2629-2015.

Davies, F., Middleton, D.R. and Bozier, K.E. (2007) Urban air pollution modelling and measurements of boundary layer height. *Atmospheric Environment*, 41, 4040–4049. https://doi.org/10.1016/j.atmosenv.2007.01.015.

European Environment Agency. (2016) *Air quality in Europe – 2016 Report*. Available at: https://www.eea.europa.eu/publications/air-quality-in-europe-2016/at_download/file [Accessed 12 March 2018].

Greater London Authority. (2016) *Mayor's air quality fund*. Available at: https://www.london.gov.uk/sites/default/files/mayors_air_quality_fund_report_2016.pdf [Accessed 12 March 2018].

Granados-Muñoz, M.J., Navas-Guzmán, F., Bravo-Aranda, J.A., Guerrero-Rascado, J.L., Lyamani, H., Fernández-Gálvez, J. and Alados-Arboledas, L. (2012) Automatic determination of the planetary boundary layer height using lidar: one-year analysis over southeastern Spain. *Journal of Geophysical Research*, 117, D18208. https://doi.org/10.1029/2012JD017524.

Haeffelin, M., Angelini, F., Morille, Y., Martucci, G., Frey, S., Gobbi, G.P., Lolli, S., O'Dowd, C.D., Sauvage, L., Xueref-Rémy, I., Wastine, B. and Feist, D.G. (2012) Evaluation of mixing-height retrievals from automatic profiling lidars and ceilometers in view of future integrated networks in Europe. *Boundary-Layer Meteorology*, 143, 49–75. https://doi.org/10.1007/s10546-011-9643-z.

Halios, C.H. and Barlow, J.F. (2018) Observations of the morning development of the urban boundary layer over London, UK, taken during the ACTUAL project. *Boundary-Layer Meteorology*, 166, 395–422. https://doi.org/10.1007/s10546-017-0300-z.

Haman, C.L., Lefer, B., Morris, G.A., Haman, C.L., Lefer, B. and Morris, G.A. (2012) Seasonal variability in the diurnal evolution of the boundary layer in a near-coastal urban environment. *Journal of Atmospheric and Oceanic Technology*, 29, 697–710. https://doi.org/10.1175/JTECH-D-11-00114.1.

van der Kamp, D. and McKendry, I. (2010) Diurnal and seasonal trends in convective mixed-layer heights estimated from two years of continuous ceilometer observations in Vancouver, BC. *Boundary-Layer Meteorology*, 137, 459–475. https://doi.org/10.1007/s10546-010-9535-7.

Kent, C.W., Grimmond, C.S.B., Barlow, J., Gatey, D., Kotthaus, S., Lindberg, F. and Halios, C.H. (2017) Evaluation of urban local-scale aerodynamic parameters: implications for the vertical profile of wind speed and for source areas. *Boundary-Layer Meteorology*, 164, 183–213. https://doi.org/10.1007/s10546-017-0248-z.

Kljun, N., Calanca, P., Rotach, M.W. and Schmid, H.P. (2015) A simple two-dimensional parameterisation for Flux Footprint Prediction (FFP). *Geoscientific Model Development*, 8, 3695–3713. https://doi.org/10.5194/gmd-8-3695-2015.

Kotthaus, S. and Grimmond, C.S.B. (2014a) Energy exchange in a dense urban environment – Part I: Temporal variability of long-term observations in central London. *Urban Climate*, 10, 261–280. https://doi.org/10.1016/j.uclim.2013.10.002.

Kotthaus, S. and Grimmond, C.S.B. (2014b) Energy exchange in a dense urban environment – Part II: Impact of spatial heterogeneity of the surface. *Urban Climate*, 10, 281–307. https://doi.org/10.1016/j.uclim.2013.10.001.

Kotthaus, S. and Grimmond, C.S.B. (2018) Atmospheric boundary-layer characteristics from ceilometer measurements. Part 1: A new method to track mixed layer height and classify clouds, *Q J R Meteorol Soc* 2018, 1–14. https://doi.org/10.1002/qj.3299.

Kotthaus, S., O'Connor, E., Münkel, C., Charlton-Perez, C., Haeffelin, M., Gabey, A.M. and Grimmond, C.S.B. (2016) Recommendations for processing atmospheric attenuated backscatter profiles from Vaisala CL31 ceilometers. *Atmospheric Measurement Techniques*, 9, 3769–3791. https://doi.org/10.5194/amt-9-3769-2016.

Lemonsu, A., Bastin, S., Masson, V. and Drobinski, P. (2006) Vertical structure of the urban boundary layer over Marseille under sea-breeze conditions. *Boundary-Layer Meteorology*, 118, 477–501. https://doi.org/10.1007/s10546-005-7772-y.

Lotteraner, C. and Piringer, M. (2016) Mixing-height time series from operational ceilometer aerosol-layer heights. *Boundary-Layer Meteorology*, 161, 265–287. https://doi.org/10.1007/s10546-016-0169-2.

Met Office. (2008) *AMDAR (Aircraft Meteorological Data Relay) reports collected by the Met Office MetDB System*. Harwell: NCAS British Atmospheric Data Centre. Available at: http://catalogue.ceda.ac.uk/uuid/33f44351f9ceb09c495b8cef74860726.

Met Office. (2012) *Met Office Integrated Data Archive System (MIDAS) land and marine surface stations data (1853–current)*. Harwell: NCAS British Atmospheric Data Centre. Available at: http://badc.nerc.ac.uk/browse/badc/ukmomidas [Accessed 12 March 2018].

Mittal, L., Baker, T., and Fuller, G. (2016) *London air quality network summary report 2014*. Available at: https://www.londonair.org.uk/london/reports/2014_LAQN_Summary_Report.pdf [Accessed 12 March 2018].

Münkel, C., Eresmaa, N., Räsänen, J. and Karppinen, A. (2007) Retrieval of mixing height and dust concentration with lidar ceilometer. *Boundary-Layer Meteorology*, 124, 117–128. https://doi.org/10.1007/s10546-006-9103-3.

Onomura, S., Grimmond, C.S.B., Lindberg, F., Holmer, B. and Thorsson, S. (2015) Meteorological forcing data for urban outdoor thermal comfort models from a coupled convective boundary layer and surface energy balance scheme. *Urban Climate*, 11, 1–23. https://doi.org/10.1016/j.uclim.2014.11.001.

Office for National Statistics. (2017) *Population Estimates for UK, England and Wales, Scotland and Northern Ireland: Mid-2016*. https://www.ons.gov.uk/releases/populationestimatesforukenglandandwalesscotlandandnorthernirelandmid2016 [Accessed 12 March 2018].

Pal, S. and Haeffelin, M. (2015) Forcing mechanisms governing diurnal, seasonal, and interannual variability in the boundary layer depths: five years of continuous lidar observations over a suburban site near Paris. *Journal of Geophysical Research: Atmospheres*, 120, 11936–11956. https://doi.org/10.1002/2015JD023268.

Pal, S., Haeffelin, M. and Batchvarova, E. (2013) Exploring a geophysical process-based attribution technique for the determination of the atmospheric boundary layer depth using aerosol lidar and near-surface meteorological measurements. *Journal of Geophysical Research: Atmospheres*, 118, 9277–9295. https://doi.org/10.1002/jgrd.50710.

Pandolfi, M., Martucci, G., Querol, X., Alastuey, A., Wilsenack, F., Frey, S., O'Dowd, C.D. and Dall'Osto, M. (2013) Continuous atmospheric boundary layer observations in the coastal urban area of Barcelona during SAPUSS. *Atmospheric Chemistry and Physics*, 13, 4983–4996. https://doi.org/10.5194/acp-13-4983-2013.

Peng, J., Grimmond, C.S.B., Fu, X., Chang, Y., Zhang, G., Guo, J., Tang, C., Gao, J., Xu, X. and Tan, J. (2017) Ceilometer based analysis of Shanghai's boundary layer height (under rain and fog free conditions). *Journal of Atmospheric and Oceanic Technology*, 34, 749–764. https://doi.org/10.1175/JTECH-D-16-0132.1.

Petäjä, T., Järvi, L., Kerminen, V.-M., Ding, A.J., Sun, J.N., Nie, W., Kujansuu, J., Virkkula, A., Yang, X., Fu, C.B., Zilitinkevich, S. and Kulmala, M. (2016) Enhanced air pollution via aerosol–boundary layer feedback in China. *Scientific Reports*, 6, 18998. https://doi.org/10.1038/srep18998.

R Core Team. (2017) *R: a language and environment for statistical computing*. Vienna: R Foundation for Statistical Computing. Available at: https://www.R-project.org/. [Accessed 12 March 2018].

The Royal College of Physicians. (2016) *Every Breath we take: the lifelong impact of air pollution*. Available at: https://www.rcplondon.ac.uk/file/2912/download?token=rhEZPBDl [Accessed 12 March 2018].

Schäfer, K., Wagner, P., Emeis, S., Jahn, C., Muenkel, C., and Suppan, P., (2012) Mixing layer height and air pollution levels in urban area, in: Kassianov, E.I., Comeron, A., Picard, R.H., Schäfer, K., Singh, U.N., Pappalardo, G. (Eds.), Society of Photo-Optical Instrumentation Engineers (SPIE) Conference Series. p. 853409. https://doi.org/10.1117/12.974328.

Schween, J.H., Hirsikko, A., Löhnert, U. and Crewell, S. (2014) Mixing-layer height retrieval with ceilometer and Doppler lidar: from case studies to long-term assessment. *Atmospheric Measurement Techniques*, 7, 3685–3704. https://doi.org/10.5194/amt-7-3685-2014.

Sicard, M., Pérez, C., Rocadenbosch, F., Baldasano, J.M. and García-Vizcaino, D. (2006) Mixed-layer depth determination in the Barcelona Coastal Area from regular lidar measurements: methods, results and limitations. *Boundary-Layer Meteorology*, 119, 135–157. https://doi.org/10.1007/s10546-005-9005-9.

Sokół, P., Stachlewska, I., Ungureanu, I. and Stefan, S. (2014) Evaluation of the boundary layer morning transition using the CL-31 ceilometer signals. *Acta Geophysica*, 62, 367–380. https://doi.org/10.2478/s11600-013-0158-5.

Stachlewska, I.S., Piądłowski, M., Migacz, S., Szkop, A., Zielińska, A.J. and Swaczyna, P.L. (2012) Ceilometer observations of the boundary layer over Warsaw, Poland. *Acta Geophysica*, 60, 1386–1412. https://doi.org/10.2478/s11600-012-0054-4.

Sun, T., Grimmond, C.S.B. and Ni, G.-H. (2016) How do green roofs mitigate urban thermal stress under heat waves? *Journal of Geophysical Research: Atmospheres*, 121, 5320–5335. https://doi.org/10.1002/2016JD024873.

Tang, G., Zhang, J., Zhu, X., Song, T., Münkel, C., Hu, B., Schäfer, K., Liu, Z., Zhang, J., Wang, L., Xin, J., Suppan, P. and Wang, Y. (2016) Mixing layer height and its implications for air pollution over Beijing, China. *Atmospheric Chemistry and Physics*, 16, 2459–2475. https://doi.org/10.5194/acp-16-2459-2016.

Visser, S., Slowik, J.G., Furger, M., Zotter, P., Bukowiecki, N., Dressler, R., Flechsig, U., Appel, K., Green, D.C., Tremper, A.H., Young, D.E., Williams, P.I., Allan, J.D., Herndon, S.C., Williams, L.R., Mohr, C., Xu, L., Ng, N.L., Detournay, A., Barlow, J.F., Halios, C.H., Fleming, Z.L., Baltensperger, U. and Prévôt, A.S.H. (2015) Kerb and urban increment of highly time-resolved trace elements in PM10, PM2.5 and PM1.0 winter aerosol in London during ClearfLo 2012. *Atmospheric Chemistry and Physics*, 15, 2367–2386. https://doi.org/10.5194/acp-15-2367-2015.

Wagner, P. and Kuttler, W. (2014) Biogenic and anthropogenic isoprene in the near-surface urban atmosphere – a case study in Essen, Germany. *Science of the Total Environment*, 475, 104–115. https://doi.org/10.1016/j.scitotenv.2013.12.026.

Wagner, P. and Schäfer, K. (2017) Influence of mixing layer height on air pollutant concentrations in an urban street canyon. *Urban Climate*, 22, 64–79. https://doi.org/10.1016/j.uclim.2015.11.001.

Ward, H.C., Kotthaus, S., Grimmond, C.S.B., Bjorkegren, A., Wilkinson, M., Morrison, W.T.J., Evans, J.G., Morison, J.I.L. and Iamarino, M. (2015) Effects of urban density on carbon dioxide exchanges: observations of dense urban, suburban and woodland areas of southern England. *Environmental Pollution*, 198, 186–200. https://doi.org/10.1016/j.envpol.2014.12.031.

Wiegner, M., Emeis, S., Freudenthaler, V., Heese, B., Junkermann, W., Münkel, C., Schäfer, K., Seefeldner, M. and Vogt, S. (2006) Mixing layer height

over Munich, Germany: variability and comparisons of different methodologies. *Journal of Geophysical Research*, 111, D13201. https://doi.org/10.1029/2005JD006593.

Wood, C.R., Lacser, A., Barlow, J.F., Padhra, A., Belcher, S.E., Nemitz, E., Helfter, C., Famulari, D. and Grimmond, C.S.B. (2010) Turbulent flow at 190 m height above London during 2006–2008: a climatology and the applicability of similarity theory. *Boundary-Layer Meteorology*, 137, 77–96. https://doi.org/10.1007/s10546-010-9516-x.

Yang, D., Li, C., Lau, A.K.-H. and Li, Y. (2013) Long-term measurement of daytime atmospheric mixing layer height over Hong Kong. *Journal of Geophysical Research: Atmospheres*, 118, 2422–2433. https://doi.org/10.1002/jgrd.50251.

Zhang, Y., Seidel, D.J. and Zhang, S. (2013) Trends in planetary boundary layer height over Europe. *Journal of Climate*, 26, 10071–10076. https://doi.org/10.1175/JCLI-D-13-00108.1.

SUPPORTING INFORMATION

Additional supporting information may be found online in the Supporting Information section at the end of the article.

How to cite this article: Kotthaus S, Grimmond CSB. Atmospheric boundary-layer characteristics from ceilometer measurements. Part 2: Application to London's urban boundary layer. *Q J R Meteorol Soc* 2018;144:1511–1524. https://doi.org/10.1002/qj.3298